45 APPLICATION OF THE IMMERSED BOUNDARY METHOD TO SIMULATIONS OF FLOW OVER STEEP, MOUNTAINOUS TERRAIN

Jason S. Simon[1*], Katherine A. Lundquist[2] and Fotini K. Chow[1]
[1] Civil and Environmental Engineering, University of California, Berkeley, California
[2] Computational Engineering Division, Lawrence Livermore National Laboratory, Livermore, California

1. INTRODUCTION

Mesoscale models like the Weather Research and Forecasting (WRF) model are traditionally used for predictions of atmospheric flow at regional scales. For higher-resolution, microscale simulations, computational fluid dynamics (CFD) codes are frequently used with the large-eddy simulation (LES) technique. Generally, mesoscale codes solve the Reynolds-averaged Navier-Stokes (RANS) equations with features for operational weather prediction and extensive parameterization schemes for atmospheric physics processes. Traditional mesoscale codes also use a terrain-following coordinate system, where the bottom boundary of the grid is mapped to the terrain and metric terms arise from the coordinate transformation. This makes the application of the bottom boundary condition straightforward and works well at resolutions too coarse to resolve the more complex features of the terrain. Terrain-following coordinate systems generate some numerical errors in the presence of any slope due to the discretized metric terms (Janjic 1977; Klemp et al. 2003). For low slopes this error is negligible but at high slopes model errors become large and can cause stability problems (Lundquist et al. 2010b). On the other hand, traditional CFD codes that are used for high-resolution studies of microscale atmospheric dynamics often have simplistic boundary conditions and do not use atmospheric physics parameterizations. The trade-off is that CFD codes, and specifically LES codes, are able to resolve turbulent eddies and thus study their evolution in the atmospheric boundary layer (ABL). These models can handle complex terrain well through use of conformal grid generation techniques, which are not terrain-following. For ABL simulations, the massive historical cost of computing resources has meant that mesoscale codes cannot be run at high resolutions if they are to cover a sufficiently large geographic region and LES codes cannot be run for large geographic regions if they are to be sufficiently resolved. A model capable of representing a range of scales is needed to seamlessly integrate from the meso to the microscale. This work continues development of such a framework, using the WRF model. WRF is both a capable mesoscale model and LES model, and is widely used for both operational and research applications (Skamarock et al. 2008). WRF is able to nest between mesoscale and LES domains, albeit in a terrain-following coordinate system. Thus, WRF in its standard form is unable to handle very steep and complex terrain at fine resolutions. An immersed boundary method (IBM) has been implemented into WRF to allow for complex terrain to be represented at high resolutions within the WRF model (Lundquist et al. 2010a, 2012). IBM immerses the terrain boundary within a non-conforming grid, using interpolation methods to represent the effect of the boundary on the flow. The difference between the grids for each coordinate system is illustrated in Figure 1. The IBM-WRF framework is an excellent candidate for a model which can capture meso and microscales over steep and complex terrain. At coarse resolutions, the terrain-following coordinates native to WRF are appropriate, but at fine resolutions over complex terrain these break down and the IBM feature is needed to represent the terrain. For a framework which uses grid nesting from meso to fine scales, the appropriate transition zone from terrain-following to IBM coordinates must be determined. In this manuscript we present three simple experiments conducted on two-dimensional domains to compare WRF and IBM-WRF and evaluate how they each perform for different grid scales. (We use "WRF" to indicate the traditional form of WRF using terrain-following coordinates and "IBM-WRF" to indicate the use of the IBM coordinates.) These preliminary results will be used to guide more costly efforts to describe the relationship between WRF and IBM-WRF in three dimensions. The experiments are designed to illustrate the numerical errors associated with both the terrain-following coordinates and the IBM coordinates and design a strategy to mitigate these errors by appropriately transitioning between WRF and IBM-WRF.

2. MATERHORN

This work is done as part of the MATERHORN campaign. The general goal of MATERHORN is to study the predictability of meteorological events in complex, mountainous terrain. The MATERHORN observational campaign will take place at the Granite Mountain Atmospheric Science Testbed

* *Corresponding author address:* Jason S. Simon, Univ. of California Berkeley, Dept. of Civil and Environmental Engineering, Berkeley, CA 94720-1710; e-mail: jasonsimon@berkeley.edu

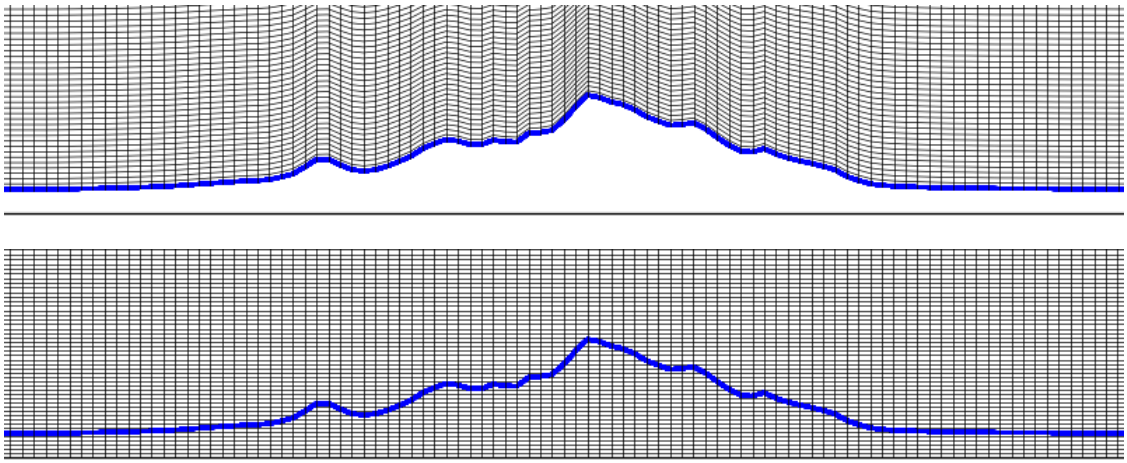

FIG. 1. A profile of Granite Mountain represented in terrain-following (top) and IBM coordinate systems. Note the distortion of grid cells near the surface when using terrain-following coordinates. At the top of the domain the terrai-following coordinates are flat. Domains are zoomed in horizontally and vertically.

FIG. 2. Approximate location of Granite Mountain (red dot). Map data ©2012 Google.

(GMAST), located at Dugway Proving Ground in Utah. Granite Mountain is a relatively isolated mountain on the playa, southwest of the Great Salt Lake (Figure 2). This creates a nearly ideal topography of a complex mountain sitting on otherwise flat topography. Figure 1 shows a line profile of an east-west cross-section of Granite Mountain and illustrates the complexity of the surface.

3. IMMERSED BOUNDARY METHOD

IBM is used to represent the effects of boundaries on non-conforming, structured grids. There are many possible implementations of IBM. As implemented, IBM-WRF uses a direct forcing method, where solutions at nodes near the boundary are calculated specifically to enforce the boundary condition. IBM-WRF applies forcing at ghost nodes (nodes that take a value only to enforce a correct solution in an adjacent node, and are not included in the physical solution) located just below the boundary. All nodes below the boundary are referred to as solid nodes, whether they are a ghost node or not. Prognostic variables are reconstructed on the ghost node by finding a fit between the ghost node, the boundary condition and the image point (reflection of the ghost node across the boundary). The value of the image point is found via interpolation from surrounding nodes in the fluid domain. In this work, the image point is found using a bilinear reconstruction scheme for two-dimensional terrain. A three-dimensional trilinear interpolation method and an inverse distance weighting method have both been implemented in IBM-WRF (Lundquist et al. 2012). An illustrative schematic of this method is shown in Figure 3. A detailed description of the implementation of IBM-WRF is presented by Lundquist (2010).

4. HYPOTHESIS AND EXPERIMENTS

The mesoscale model WRF uses a terrain-following coordinate system. As previously discussed, this becomes an issue in steep topography. Terrain data is often available at very high resolutions ($\sim$5m), therefore the steepness of the terrain represented in the model is essentially determined by the horizontal resolution of the simulation. Thus, we assume that the numerical errors due to WRF's coordinate system increase as the grid spacing decreases, provided steep terrain is present and no adjustments are being made to the vertical resolution (Mahrer 1984). IBM-WRF, on the other hand, relies on interpolation at the terrain boundary. Therefore, when modeling complex terrain at the mesoscale, terrain-following coordinates are preferable because the numerical errors from the coordinate transformation are smaller than the numerical

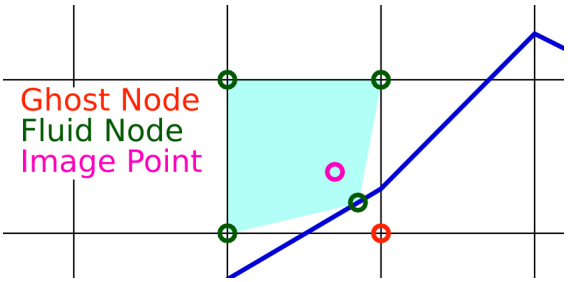

FIG. 3. Visual description of the three types of nodes used in IBM-WRF. The blue line represents the terrain surface. The ghost node is the first node beneath the surface, and its image point is a reflection normal to the surface into the fluid domain. The green fluid nodes mark the values that are interpolated to find the image point value. The image point value and the boundary condition determine the value that the ghost node takes. In this example the value at the boundary is used, which is the case only under Dirichlet boundary conditions.

errors introduced by the interpolation scheme. Once the grid spacing is larger than the terrain scale, the surface is approximately flat and IBM-WRF's interpolation is adequate. This creates numerical error inherent in IBM-WRF that is very low at high resolutions, regardless of the presence of steep terrain, and high at coarse resolutions in the presence of steep terrain. At the point where the terrain is coarse enough to be essentially flat the error returns to a low value. While the performance of terrain-following coordinates in steep terrain is well studied (Janjic 1977, 1989; Klemp et al. 2003; Schär et al. 2002; Zängl 2002, 2003, 2004; Zängl et al. 2004), the horizontal resolutions appropriate for WRF and IBM-WRF relative to each other are not known. Given the inverse effect of resolution on the numerical errors of the two coordinate systems, when nesting from coarse to fine domains in an IBM-WRF framework, there should exist a horizontal resolution where the modeler is best served by changing from WRF to IBM-WRF. A simple analysis of the relationship between the two models and horizontal resolution (and thus, indirectly, slope) can be done to estimate the nature of the two models' appropriate spatial scales. Figure 4 shows a schematic of the expected numerical errors of each coordinate system compared to a hypothetical exact solution. It follows that, if the shapes are correct, the difference between the solutions from WRF and IBM-WRF should relatively follow the sum of the two individual curves, and the resolution to switch from WRF to IBM-WRF should be the point where the two curves intersect. Note that in this schematic of the error curve WRF is shown to have a value across the entire spectrum of resolutions, and indeed this is how we expect the theoretical error associated with terrain-following coordinates to behave. In reality, though, WRF will have stability problems at very steep slopes (fine resolutions) and the error will not be measurable.

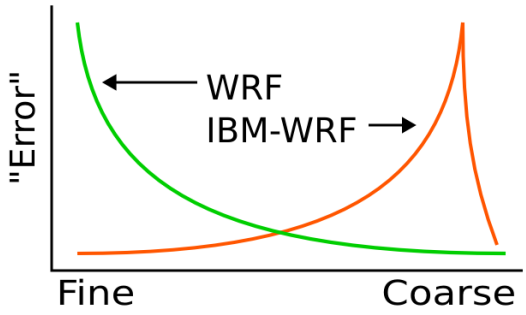

FIG. 4. Schematic of expected behavior of numerical error in WRF and IBM-WRF as a function of horizontal grid resolution.

5. DIFFERENCE VS. HORIZONTAL RESOLUTION

To estimate the behavior of the numerical error, WRF and IBM-WRF are run in complex terrain at different horizontal resolutions to compare differences in the resulting velocities. The terrain being used is an idealization of Granite Mountain created by prescribing a minimum elevation in the domain and removing all features other than the mountain. The result is an isolated mountain on a perfectly flat playa, which is a relatively realistic representation at the microscale. A two-dimensional east-west slice is taken through one of the highest points on Granite Mountain. The solutions from WRF and IBM-WRF are compared by interpolating the velocity magnitude field from IBM-WRF to the terrain-following coordinate system and taking the difference at each node in the domain. The difference between the two coordinate systems is represented by the largest difference, in magnitude, present in the domain. For convenience, hereafter this interpolated velocity difference field between WRF and IBM-WRF will simply be referred to as the difference and will be a surrogate for the theoretical error in the system. This assumes that for any horizontal resolution one of the coordinate systems is appropriate and can give an accurate solution.

a. MODEL SETUP

All cases are two-dimensional in the east-west direction with 50 horizontal grid points. The horizontal resolutions used range from 450m to 4km. These extents were found empirically. The finest grid is determined by the point where WRF becomes numerically unstable for this configuration, and the coarsest grid is the point where the difference between WRF and IBM-WRF starts decreasing. WRF has 90 vertical grid points, covering a vertical span from 1315m to 7000m above sea-level (ASL). IBM-WRF has 92 vertical grid points, to account for the two necessary solid nodes below the ter-

rain, and covers a vertical span from 1215m to 7000m ASL. The cases are run for 6 hours with a 0.25s timestep, with 5m/s geostrophic forcing. The initial temperature profile is neutral and the initial velocity profile is a uniform 5m/s westerly flow. The eddy viscosity for all cases is $100m^2/s$, to allow the solution to reach steady-state quickly. Coriolis is neglected. A no-slip bottom boundary condition implemented by Lundquist et al. (2010a) is used and a Rayleigh damping layer is present at the top 2km of the grid. The lateral boundary conditions are periodic. Terrain data is obtained from the Utah AGRC's 5m Auto-Correlated Digital Elevation Model (DEM) with aforementioned adjustments; minimum elevation has been set to 1315m. The DEM is interpolated to the model domain using the WRF Preprocessing System's (WPS) average grid cell interpolation and smoothing-desmoothing. Of the aforementioned settings, the results are most sensitive to vertical resolution and eddy viscosity.

b. RESULTS

Figure 5 shows the maximum difference of five representative resolutions. The figures have a horizontal span of 60km, centered on Granite Mountain, and extend vertically to 4km ASL (from a base of 1315m). In all cases the maximum difference is on the lee side of the mountain and spreads downstream. The general trend is illustrated in these cases: the largest error is present in the 3km domain, with a decreasing trend in either direction. Notice that in the coarsest case the error is centered on the downstream edge of the mountain and spreads downstream, while in the finer two cases the error is located more directly over the mountain and does not spread nearly as far. The extreme cases appear to have a different mechanism causing their respective differences. Figure 6 shows the maximum difference as a function of grid spacing. The error increases at coarser resolutions, as expected. With coarser grids, the terrain slope is lower, hence the WRF solution does a better job. The increase in error is due to interpolation errors in the IBM-WRF solution, which become larger at coarse resolution because the distance between grid points increases. Thus, the shape seen is approximately what we would expect to see if only evaluating the error from IBM-WRF. Once the resolution is so coarse that the terrain looks entirely flat to the model, the difference between the results becomes quite small, leading to a sharp drop-off in the curve at very coarse resolutions. These results therefore capture the orange curve in the Figure 4 schematic above. The green curve requires very fine resolutions where WRF may not be able to accurately run, especially in two dimensions.

6. DIFFERENCE VS. SLOPE

The previous experiment was conducted at coarse resolutions where IBM-WRF has not previously been tested (because it was not designed for such coarse resolutions). At these coarse resolutions, the above results imply that the terrain-following coordinates are more accurate than using IBM. The difference between the models is dominated by the effects of grid spacing on IBM-WRF, and it is very difficult to discern the impact that the slope has on WRF. The point where slope issues begin to dominate is of great interest, since it likely plays a large role in defining the edge of both WRF and IBM-WRF's preferred scale ranges. The scale that is dominated by terrain slopes is not present due to numerical limitations. Since this is a two-dimensional domain it should not be assumed that horizontal resolutions that are too fine for WRF under these settings remain problematic in more realistic, three-dimensional cases. A second experiment is conducted to evaluate the relationship between slope and error. The horizontal resolution remains constant at 500m and the terrain is scaled from zero to one. The scaling factor is applied only to heights above the artificial floor of the topography. When the scale is zero, our domain is reduced to flat terrain and the two coordinate systems should yield nearly identical results. When the scale is one, we know from our first experiment that the maximum difference for this setup at 500m horizontal resolution should be approximately 0.6m/s (Figure 6). Since the resolution here is not changing, the variability in the error associated with grid points catching peaks and troughs in the terrain is not in play, and thus the trend should be very clear.

a. MODEL SETUP

The setup from the first experiment for 500m horizontal resolution is scaled to coefficients of 0, 0.1, 0.2, 0.4, 0.6, 0.8 and 1.0. Since such strong trends are produced by this experiment, it is conducted for different eddy viscosities as well (K=20, 30, 40, 50, $100m^2/s$). All other settings are consistent throughout all runs. The coefficients used for each resolution are shown in Figure 7.

b. RESULTS

Figure 8 shows five of the seven terrain scales (for K = $100m^2/s$) and their difference field. A clear pattern, focused just on the lee side of the peak, emerges as the height of the mountain is increased. Even in the least dramatic case, the location of the mountain can be made out easily by the location of nonzero difference values. The maximum difference values seen in each domain, and for each eddy viscosity, follow a very strong increasing trend with slope. In Figure 9 the maximum differences are plotted against slope, with the slope axis reversed to mimic the pattern that would emerge were grid spacing used on the independent axis. Despite the altering of the x-axis, Figure 9 closely resembles the green curve in Figure 4 above. This experiment is the only of the ones presented to vary eddy viscosity (all values are included in Figure 9). When the eddy viscosity is high the parameterized turbulent mixing is rapid and velocity fluctuations are smoothed out. Thus the expected result is that for any scenario, a larger eddy viscosity

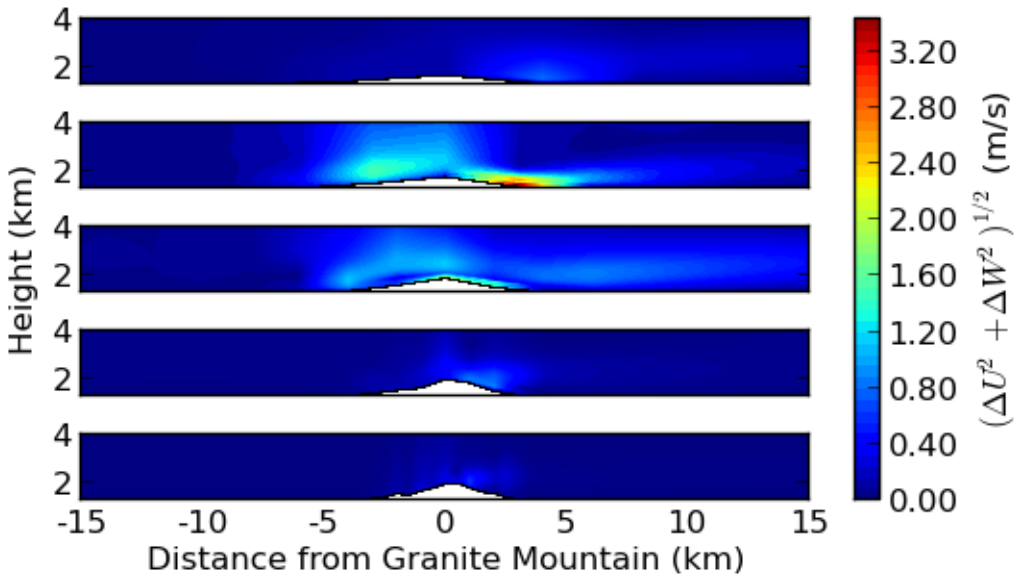

FIG. 5. Sample of velocity magnitude difference fields from the first experiment. Cases where the horizontal resolution is (from top to bottom) 4km, 3km, 2km, 1km and 500m. Only horizontal resolution is actively changed for the different cases. Domains are zoomed in horizontally and vertically. To scale.

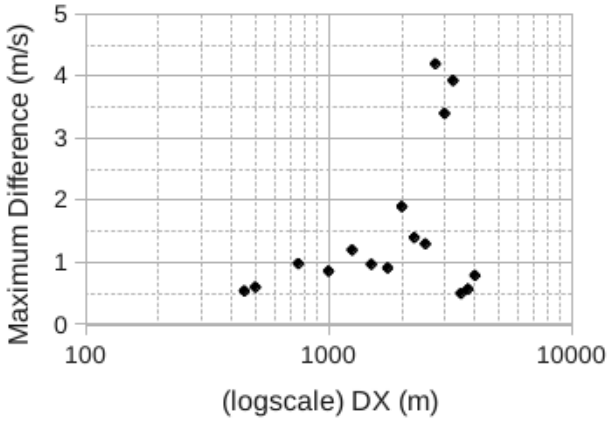

FIG. 6. Maximum nodal difference in velocity magnitude between WRF and IBM-WRF (interpolated to WRF's grid) in the first experiment. Only horizontal resolution is actively changed for the different cases. Semi-log scale.

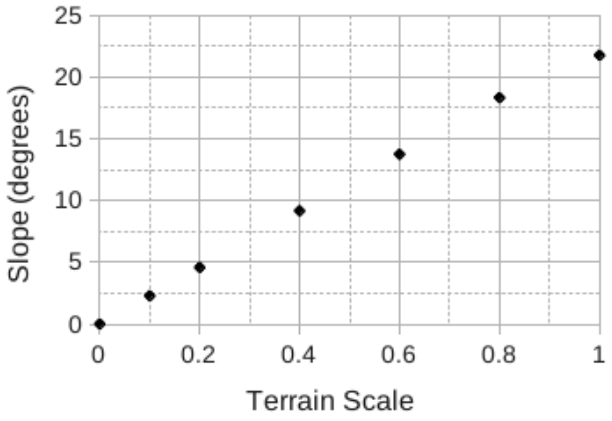

FIG. 7. Scales used on the terrain to achieve different slopes in the second experiment. Horizontal resolution is 500m for all cases.

will always yield a smaller maximum error. This was indeed the case for these results.

7. DIFFERENCE VS. GRID SPACING

In the first experiment a strong relationship between horizontal resolution and difference is seen. Horizontal resolution in this case, though, is essentially two variables: grid spacing and slope, and the different effects of the two are difficult to de-couple. To make this distinction, grid spacing is examined alone. In this experiment 19 different horizontal resolutions between 4km and 450m are used. For each resolution, the height of Granite Mountain is scaled so that the maximum slope seen over any set of adjacent grid point is 10 degrees. All other factors remain constant. This allows for different grid spacings to be evaluated without an associated decrease in slope.

a. MODEL SETUP

The base model setup the same as the previous case, with a scaling factor used to maintain a maximum slope of 10 degrees at each resolution. Figure 10 shows the scales used at each resolution to achieve the necessary maximum slope.

b. RESULTS

Difference fields for five representative domains are shown in Figure 11. Unlike in Figure 8, where the difference seems to emerge directly from the mountain, the differences here are much more sporadic and concentrated to the sides of the mountain. Such patterns, especially the one shown for the 2km case, indicate an interpolation error in IBM-WRF. This is visually confirmed in Figure 12 by comparing the velocity magnitude fields of WRF and IBM-WRF. The resulting relationship between maximum difference and horizontal resolution is shown in Figure 13. The difference follows a similar trend as the initial experiment, but shows no sign of a low-valued tail. Two outliers are very visible (noted in Figure 13), but the trend is clearly present. Interestingly, the outliers are both at horizontal resolutions where the scaling factor is < 1, which is counter-intuitive. A decrease in the scale of the terrain is expected to be accompanied by an improvement in mutual agreement between the two systems. These outliers seem to be a result of a variable nature possessed by IBM-WRF at coarse resolutions, and are an example of an issue that the implementation of a log-law could potentially address.

8. CONCLUDING REMARKS

The combined WRF and IBM-WRF framework is potentially a very powerful atmospheric model, capable of ranging across essentially all scales of the globe. The meso-to-micro scale nesting capability would allow for LES at the finest scales to consider regional weather effects associated with observational data. This would allow improved capabilities for joint observational and modeling studies of the atmosphere, especially studies of atmospheric turbulence. The general spatial scale where each coordinate system is appropriate is known, however the specific nature of numerical errors in the different systems is not known. If these two systems are to be used in a single modeling framework, the nature of the two systems relative to each other and their model settings must be investigated in more detail. In this work we have presented a model for the behavior of numerical errors from WRF's terrain-following coordinate system and IBM-WRF's immersed boundary method and conducted three simple experiments to evaluate this model. An expected result is that for fine resolutions (and steep slopes) there is a large difference between the dynamics of WRF and IBM-WRF. A large difference is also expected at coarse resolutions, with a range of moderate resolutions that show noted agreement. The expected relationship at coarse resolutions was confirmed. For very fine resolutions the relationship could not be verified due to numerical instabilities, so the difference between WRF and IBM-WRF was evaluated for increasing slopes at a constant resolution. Large slopes were confirmed to have a negative impact on the agreement of the models. From these results it can be concluded that the appropriate choice of coordinate system (terrain-following vs. IBM) is highly dependent on horizontal resolution and terrain slope. It is also concluded that, for two dimensions, there is a range where the difference between WRF and IBM-WRF is small; this is the located of the desired transition between the two (see Figure 4). It is expected that these results will be helpful in designing three-dimensional experiments, which will be both more expensive and less dynamically constrained. The errors generated by terrain-following coordinates in WRF are a result of truncation errors which become large over very steep slopes. The errors generated by IBM-WRF are primarily a result of inaccurate interpolation caused by large spatial distances between grid points. This interpolation error can partially be alleviated with the implementation of a log-law to reconstruct image point values. Indeed, this is a subject of ongoing work that is expected to increase the flexibility of IBM-WRF to extend to coarser resolutions.

9. ACKNOWLEDGEMENTS

This research was funded by Office of Naval Research Award #N00014-11-1-0709, Mountain Terrain Atmospheric Modeling and Observations (MATERHORN) Program.

10. REFERENCES

Janjic, Z. I., 1977: Pressure gradient force and advection scheme used for forecasting with steep and small scale topography. *Beitr. Phys. Atmos.*, **50**, 186–189.

Janjic, Z. I., 1989: On the pressure gradient force error in σ

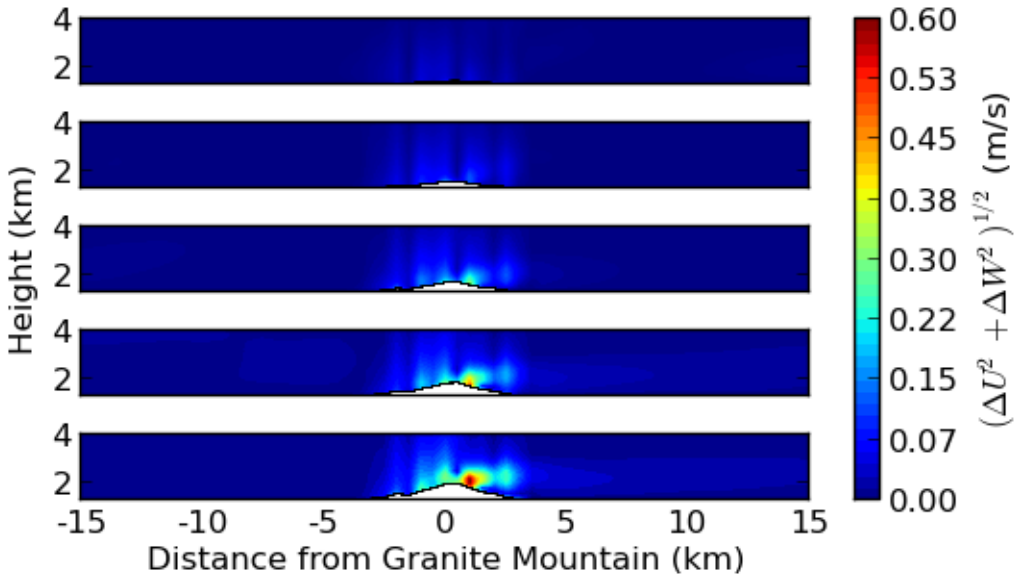

FIG. 8. Sample of velocity magnitude difference fields from the second experiment. Cases where the terrain scale is (from top to bottom) 0.2, 0.4, 0.6, 0.8, 1.0. Horizontal resolution is 500m for all cases and the terrain is scaled to change the steepness. Domains are zoomed in horizontally and vertically. To scale.

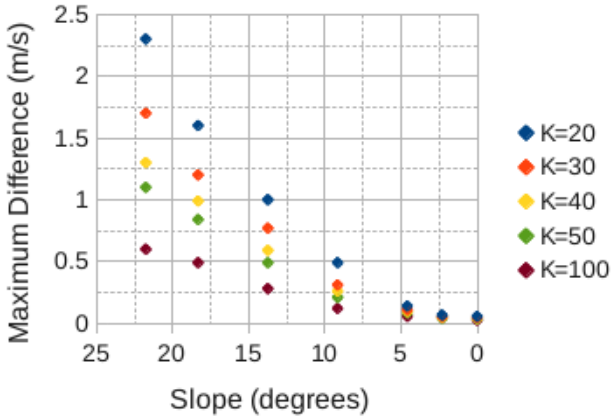

FIG. 9. Maximum nodal difference in velocity magnitude between WRF and IBM-WRF (interpolated to WRF's grid) in the second experiment, as a function of slope. Slope is plotted in reverse to mimic the shape expected when grid spacing is the independent variable. Horizontal resolution is 500m for all cases and the terrain is scaled to change the steepness.

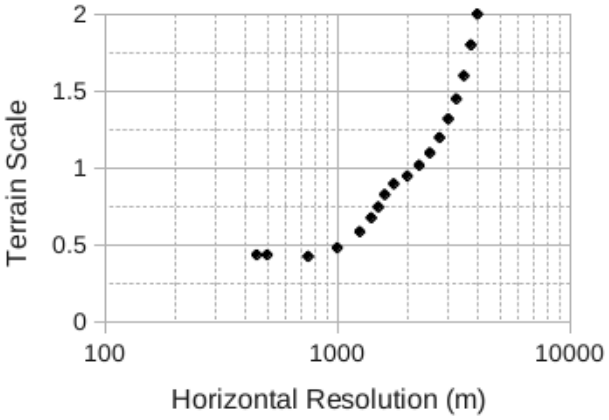

FIG. 10. Scales used on the terrain to achieve a maximum slope of 10 degrees for each case of varying horizontal resolution. Semi-log scale.

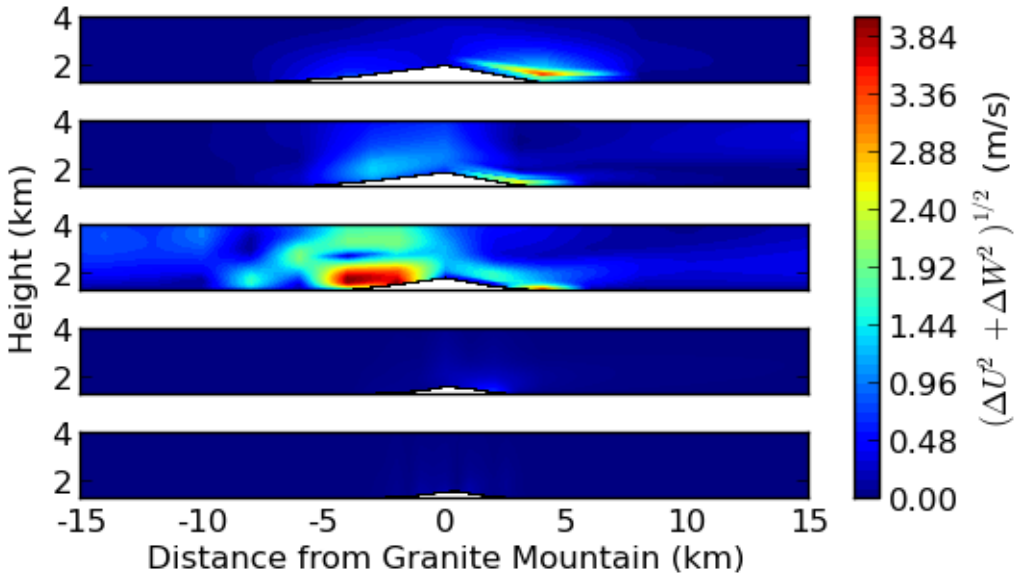

FIG. 11. Sample velocity magnitude difference fields from the third experiment. Cases where the horizontal resolution is (from top to bottom) 4km, 3km, 2km, 1km, 500m. The terrain is scaled so that the maximum slope between adjacent nodes is 10 degrees for every resolution. Domains are zoomed in horizontally and vertically. To scale.

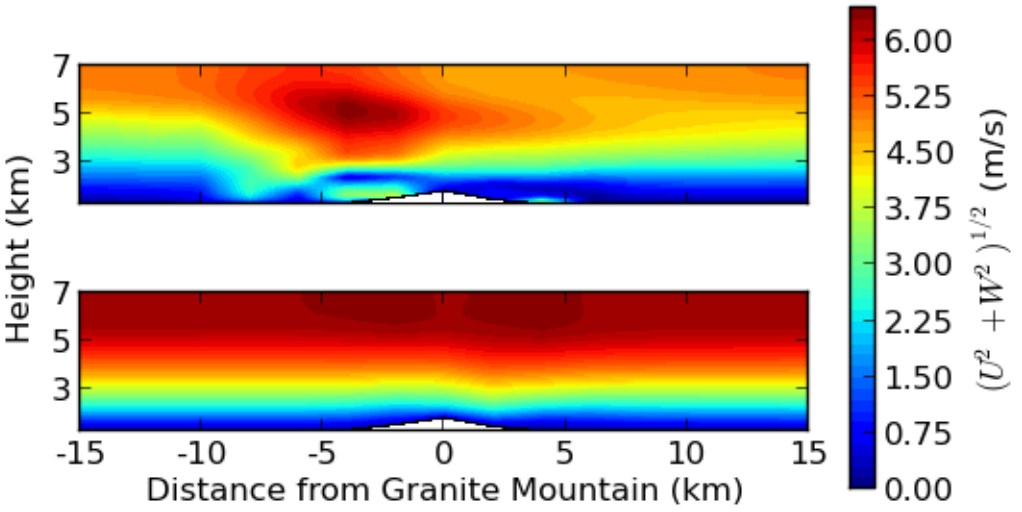

FIG. 12. Velocity magnitude fields for IBM-WRF (top) and WRF when the horizontal resolution is 2km and the maximum slope is artificially set to 10 degrees. To scale.

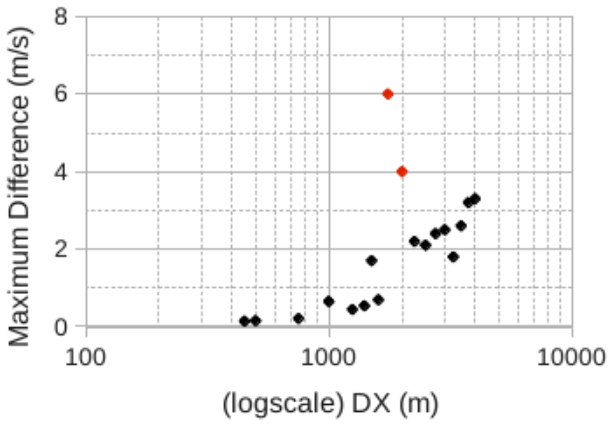

FIG. 13. Maximum nodal difference in velocity magnitude between WRF and IBM-WRF (interpolated to WRF's grid) in the third experiment. The terrain is scaled so that the maximum slope between adjacent nodes is 10 degrees for every resolution. Two outliers marked with red. Semi-log scale.

coordiante spectral models. *Mon. Wea. Rev.*, **117**, 2285–2292.

Klemp, J., W. Skamarock, and O. Fuhrer, 2003: Numerical consistency of metric terms in terrain-following coordinates. *Mon. Wea. Rev.*, **131**, 1229–1239.

Lundquist, K. A., 2010: Immersed boundary methods for high-resolution simulations of atmospheric boundary-layer flow over complex terrain. Ph.D. thesis, University of California, Berkeley.

Lundquist, K. A., F. K. Chow, and J. K. Lundquist, 2010a: An immersed boundary method for the weather research and forecasting model. *Mon. Wea. Rev.*, **138 (3)**, 796–817.

Lundquist, K. A., F. K. Chow, and J. K. Lundquist, 2010b: Numerical errors in flow over steep topography: analysis and alternatives. *14th Conference on Mountain Meteorology*, American Meteorological Society.

Lundquist, K. A., F. K. Chow, and J. K. Lundquist, 2012: An immersed boundary method enabling large-eddy simulations of flow over complex terrain in the wrf-model. *Mon. Wea. Rev.*, in press.

Mahrer, Y., 1984: An improved numerical approximation of the horizontal gradients in a terrain-following coordinate system. *Mon. Wea. Rev.*, **112**, 918–922.

Schär, C., D. Leuenberger, O. Fuhrer, D. Lüthi, and C. Girard, 2002: A new terrain-following vertical coordinate formulation for atmospheric prediction models. *Mon. Wea. Rev.*, **130**, 2459–2480.

Skamarock, W., et al., 2008: A description of the advanced research wrf version 3. NCAR Technical Note.

Zängl, G., 2002: An improved method for computing horizontal diffusion in a sigma-coordinate model and its application to simulations over mountainous topography. *Mon. Wea. Rev.*, **130**, 1423–1432.

Zängl, G., 2003: A generalized sigma-coordinate system for the mm5. *Mon. Wea. Rev.*, **131**, 2875–2884.

Zängl, G., 2004: The sensitivity of simulated orographic precipitation to model components other than cloud microphysics. *Q. J. R. Meterol. Soc.*, **130**, 1857–1875.

Zängl, G., L. Gantner, G. Hartjenstein, and H. Noppel, 2004: Numerical errors above steep topography: A model intercomparison. *Meteorol. Z.*, **13**, 69–76.